All-charm tetraquark in front form dynamics

Zhongkui Kuang (邝中奎),[1,2,3,*] Kamil Serafin,[1,2,†] Xingbo Zhao,[1,2,3,‡] and James P. Vary[4,§]

(BLFQ Collaboration)

[1]*Institute of Modern Physics, Chinese Academy of Sciences, Lanzhou 730000, China*
[2]*CAS Key Laboratory of High Precision Nuclear Spectroscopy, Institute of Modern Physics, Chinese Academy of Sciences, Lanzhou 730000, China*
[3]*School of Nuclear Science and Technology, University of Chinese Academy of Sciences, Beijing 100049, China*
[4]*Department of Physics and Astronomy, Iowa State University, Ames, Iowa 50011, USA*

(Received 20 January 2022; accepted 5 May 2022; published 24 May 2022)

We study all-charm tetraquarks in the front form of Hamiltonian dynamics using the many-body basis function approach known as basis light-front quantization. The model Hamiltonian contains transverse and longitudinal confining potentials and a one-gluon-exchange effective potential. We calculate masses of two-charm-two-anticharm states focusing on the lowest state. We also calculate two-quark and four-quark estimates of meson-meson breakup threshold. The results suggest that the lowest two-charm-two-anticharm state is not a tightly bound tetraquark. We discuss implications of the cluster decomposition principle for theories formulated on the light front and present our treatment of identical particles together with color-singlet restrictions on the space of quantum states.

DOI: 10.1103/PhysRevD.105.094028

I. INTRODUCTION

Even though four-quark states called tetraquarks have been studied for a long time (see Refs. [1–4] for some early studies), the stability of tetraquarks is still under debate. One of the basic questions is whether there are four-quark states whose masses are smaller than the sum of the masses of two mesons into which the tetraquark could potentially decay through a rearrangement of the quarks. Because *ab initio* calculations in QCD are challenging, researchers make use of various strategies and approaches to estimate the masses of tetraquarks, and their results are often in conflict with each other [5–40]. The goal of our paper is to initiate studies of tetraquarks within the framework of the front form of Hamiltonian dynamics [41] and basis light-front quantization (BLFQ) [42], an approach whose ultimate goal is to achieve *ab initio* calculations in QCD. Therefore, our study is focused on the development of the approach as much as on providing a preliminary answer to the main tetraquark problem—whether or not four heavy quarks can form a bound state.

We choose to study heavy quarks (charm quarks) because for heavy quarks one would expect it to be possible for the proper, QCD-based theoretical description to be simplified. Asymptotic freedom, which is believed to be relevant for heavy quarks, allows for perturbative expansion of the QCD Hamiltonian and produces some confidence that the simple Hamiltonian with confining and one-gluon-exchange potentials that we use shares important features with the full QCD Hamiltonian. Owing to asymptotic freedom and quark masses much larger than the strong interaction scale Λ_{QCD}, charm quarks are expected to be relatively slow in comparison to the speed of light; hence, additional pairs of heavy charm quarks cannot be easily produced and should not contribute significantly to the tetraquark dynamics. Tetraquarks of any kind are an interesting topic of study because they are exotic, i.e., they are neither mesons nor baryons; therefore, they provide opportunities to test and extend our understanding of hadron physics beyond the boundary of fairly well-established meson and baryon physics. Finally, studies of all-heavy tetraquarks recently received additional motivation in the form of the first experimental identification of all-charm tetraquark resonance $X(6900)$ [43]. The discovery of a doubly charmed tetraquark is also worth noting [44].

*kuangzhongkui@impcas.ac.cn
†kserafin@impcas.ac.cn
‡xbzhao@impcas.ac.cn
§jvary@iastate.edu

BLFQ has already been used with success to study various mesons and baryons [45–54] as well as in QED; see, for example, Ref. [55]. However, most of those studies involve only one Fock sector, with recently appearing extensions [56]. Questions like "how does confinement work?" cannot be fully answered by studying quark-antiquark or three-quark systems alone, even if one uses phenomenologically successful confining potentials. If one is to believe that gluon strings are formed in a Hamiltonian approach to QCD (as seems to be the case for lattice QCD), then one is necessarily forced to explicitly include many-gluon sectors in addition to the leading "valence" Fock sector. Furthermore, breaking of those strings requires Fock sectors with additional quark-antiquark pairs. The strength of BLFQ stems from the fact that, in principle, it can handle many Fock sectors, each of which can contain many particles, in a straightforward manner.

The QCD Fock space is rich in structure and, even with the help of supercomputers, the calculations are challenging because the dimensionality of the required spaces of states grows quickly with the addition of new Fock sectors. The $Q\bar{Q}Q\bar{Q}$ sector is one of the natural next targets after the $Q\bar{Q}$ and QQQ sectors.

Another important challenge resides in how to renormalize divergent interactions of QCD. The eventual success of the approach will probably require an adoption of effective interactions calculated from QCD using, for example, the renormalization group procedure for effective particles (RGPEP) [57]. The Hamiltonian of bare, pointlike quarks and gluons leads to the problem of overlapping divergences [58]. RGPEP, by defining effective, finite-size particles, can tame singular interactions and reduce the number of Fock sectors necessary to obtain satisfactory results. Effective Hamiltonians computed using the closely related similarity renormalization group [59] (see also Ref. [60]) have been successfully used in combination with many-body methods in *ab initio* calculations in nuclear physics; see, for example, [61–63]. However, a relativistic quantum field theory such as QCD is much more complicated than the nonrelativistic nuclear many-body problem of interacting nucleons.

Since we choose to deal with only charm quarks and antiquarks, we take into account the antisymmetrization of identical particles. This is also the first system treated within BLFQ where the question about color dependence of the confining potential needs to be addressed because there are two color-singlet combinations in the $Q\bar{Q}Q\bar{Q}$ sector, whereas both the $Q\bar{Q}$ and QQQ sectors admit only one color singlet each. We adopt the commonly used assumption that the confining potential depends on color in exactly the same manner as one-gluon-exchange interactions depend on color. We also add a color-independent term in the longitudinal direction. Without this added term, we find some spurious, unphysical solutions with negative mass squared.

In Sec. II we present our model many-body Hamiltonian and derive Schrödinger-like equations for three cases describing one meson, a tetraquark, and two mesons. The two-meson system allows us to discuss the cluster decomposition principle on the light front. Section III is devoted to a description of the main elements of the computational framework of BLFQ. Our results for the masses in the three mentioned cases and a discussion about whether all-charm tetraquarks are stable against dissociation are given in Sec. IV. Section V concludes the paper. Color factors between color-singlet states are given in the Appendix, where we describe the procedure that takes into account the Pauli exclusion principle and allows us to work with color singlets only.

II. HAMILTONIAN

A. Front form of Hamiltonian dynamics

Before we introduce our model Hamiltonian, we mention a few aspects of the framework that we use that are important in the context of our long-term goal of *ab initio* calculations in QCD. The front form of Hamiltonian dynamics [41] has two important advantages over other Hamiltonian approaches. One of them is the fact that particles cannot be created from the free vacuum in a way that they can be created, for example, in the instant form of Hamiltonian dynamics. Front form theories conserve total longitudinal momentum of particles taking part in the interaction, where the longitudinal momentum of a particle is defined as $p^+ = p^0 + p^3$. In Hamiltonian approaches particles are on mass shell; hence, $p^0 \geq |p^3|$ and p^+ cannot be negative. At the same time the vacuum should have $p^+ = 0$; therefore, all particles created from the vacuum should have exactly $p^+ = 0$. Since for massive particles $p^+ \to 0$ means energy diverging to infinity, one should regularize the theory and remove the $p^+ = 0$ states, which are called zero modes. However, it is also known that one cannot simply discard those states and that zero modes have to be taken into account in some way. Even though it is an open question as to exactly which way zero modes need to be included, we have still gained something: the difference between the free vacuum and the interacting vacuum can be contained only in the singular point $p^+ = 0$. Therefore, to a large extent one can separate zero modes from the $p^+ > 0$ region, where most of the usual dynamics happen [this is similar in form to the Schrödinger equation or quark model Hamiltonians; see Eqs. (23), (28), and (36)]. This is in contradistinction with the instant form, in which particles of arbitrary momenta can be created from the free vacuum, making the interacting vacuum a complicated state upon which one-, two-, and many-particle states are to be built.

Another advantage of the front form of Hamiltonian dynamics is the fact that one can freely boost particles, and wave functions can be decomposed into products of total

and relative motion factors. This is very fortunate because one can use exactly the same wave functions that describe the internal structure of a hadron regardless of how fast the hadron is moving in the laboratory frame. Hence, the front form is uniquely suited to describing high-energy processes and offers practical advantages for building a Poincaré-covariant quantum theory in a Hamiltonian approach.

In the front form of Hamiltonian dynamics, the Hamiltonian is $P^- = P^0 - P^3$. The momentum operators are $P^+ = P^0 + P^3$, which is the longitudinal momentum, and the transverse momenta are P^1 and P^2. We denote two-dimensional transverse vectors in bold font, e.g., $\mathbf{P} = (P^1, P^2)$. The evolution of quantum states is given by the analog of the Schrödinger equation, which in the stationary version is $P^-|\Psi\rangle = E|\Psi\rangle$, where E is the eigenvalue of operator P^-. One can also study the closely related eigenvalue equation

$$P^\mu P_\mu |\Psi\rangle = M^2 |\Psi\rangle, \tag{1}$$

where the eigenvalue M^2 is the invariant mass squared of the eigenstate $|\Psi\rangle$. The eigenvalue M^2 depends only on the relative motion of the constituents and not on their absolute motion. Since we work with $P^\mu P_\mu$ instead of P^- it is convenient for us to call $H = P^\mu P_\mu$ the Hamiltonian. This is sometimes referred to as the "light cone Hamiltonian" [64]. Therefore,

$$H = P^+ P^- - \mathbf{P}^2. \tag{2}$$

In the front form of Hamiltonian dynamics operators P^+ and $\mathbf{P}$ are kinematic, while P^- is dynamic. In other words, P^- contains interactions, while P^+ and $\mathbf{P}$ are the same regardless of which interactions are present in the theory.

B. Hamiltonian

The model Hamiltonian that we use to study four-quark systems is

$$H = H_{\text{kinetic}} + H_{\text{transverse}} + H_{\text{longitudinal}} + H_{\text{OGE}}, \tag{3}$$

where H_{kinetic}, $H_{\text{transverse}}$, $H_{\text{longitudinal}}$, and H_{OGE} stand for the kinetic term, transverse confining potential term, longitudinal confining potential term, and one-gluon-exchange (OGE) term, respectively. The kinetic energy Hamiltonian is

$$H_{\text{kinetic}} = P^+ P_0^- - \mathbf{P}^2, \tag{4}$$

where P_0^- stands for the noninteracting, kinetic part of P^-. The momentum operators are

$$P^+ = \int_1 p_1^+ (b_1^\dagger b_1 + d_1^\dagger d_1), \tag{5}$$

$$\mathbf{P} = \int_1 \mathbf{p}_1 (b_1^\dagger b_1 + d_1^\dagger d_1), \tag{6}$$

$$P_0^- = \int_1 p_1^- (b_1^\dagger b_1 + d_1^\dagger d_1), \tag{7}$$

with $p_1^- = (m^2 + \mathbf{p}_1^2)/p_1^+$, where m is the quark mass and b_1 and d_1 are annihilation operators of a quark and an antiquark with label 1, respectively. Moreover,

$$\int_1 = \sum_{c_1,\sigma_1} \int_0^\infty \frac{dp_1^+}{4\pi p_1^+} \int \frac{d^2\mathbf{p}_1}{(2\pi)^2}, \tag{8}$$

where c_1 and σ_1 are the color and the light-front helicity of particle 1, respectively. The normalization of operators is $\{b_1, b_2^\dagger\} = \{d_1, d_2^\dagger\} = p_1^+ \tilde{\delta}_{1.2} \delta_{\sigma_1,\sigma_2} \delta_{c_1,c_2}$, where $\tilde{\delta}_{1.2}$ stands for the momentum conservation Dirac delta multiplied by $16\pi^3$.

The Hamiltonians of the transverse and longitudinal confining potentials are

$$H_{\text{transverse}} = \int_{121'2'} (p_1^+ + p_2^+) \tilde{\delta}_{12.1'2'} U_{\text{conf},\perp} \text{BD}_{\text{OGE}}, \tag{9}$$

$$H_{\text{longitudinal}} = \int_{121'2'} (p_1^+ + p_2^+) \tilde{\delta}_{12.1'2'} U_{\text{conf},z} [a \text{BD}_{\text{OGE}} + C_F (a-1) \text{BD}_{\text{CI}}], \tag{10}$$

where $U_{\text{conf},\perp}$ and $U_{\text{conf},z}$ are the interaction kernels that depend on the momenta and helicities of particles 1, 2, 1′, and 2′. The momentum conservation Dirac delta is

$$\tilde{\delta}_{12.1'2'} = 4\pi \delta(p_1^+ + p_2^+ - p_{1'}^+ - p_{2'}^+) \cdot (2\pi)^2 \delta^2(\mathbf{p}_1 + \mathbf{p}_2 - \mathbf{p}_{1'} - \mathbf{p}_{2'}). \tag{11}$$

The color dependence is encoded in BD_{OGE} and BD_{CI},

$$\text{BD}_{\text{OGE}} = \sum_{a=1}^{8} \left(\frac{1}{2} t_{11'}^a t_{22'}^a b_1^\dagger b_2^\dagger b_{2'} b_{1'} - t_{11'}^a t_{2'2}^a b_1^\dagger d_2^\dagger d_{2'} b_{1'} + \frac{1}{2} t_{1'1}^a t_{2'2}^a d_1^\dagger d_2^\dagger d_{2'} d_{1'} \right), \tag{12}$$

$$\text{BD}_{\text{CI}} = \delta_{c_1,c_{1'}} \delta_{c_2,c_{2'}} \left(\frac{1}{2} b_1^\dagger b_2^\dagger b_{2'} b_{1'} + b_1^\dagger d_2^\dagger d_{2'} b_{1'} + \frac{1}{2} d_1^\dagger d_2^\dagger d_{2'} d_{1'} \right), \tag{13}$$

with t_{ij}^a standing for $\chi_{c_i}^\dagger T^a \chi_{c_j}$, where $T^a = \frac{1}{2}\lambda^a$, with λ^a being a Gell-Mann matrix ($a = 1, 2, \ldots, 8$) and $\chi_c = [\delta_{c,1}, \delta_{c,2}, \delta_{c,3}]^T$ being a three-dimensional vector, while $c = 1, 2, 3$ is the color quantum number. In other words, t_{ij}^a

is half of the matrix element of matrix λ^a in the c_ith row and c_jth column. The color dependence of $\mathrm{BD}_{\mathrm{OGE}}$ is the same as the color dependence of the one-gluon exchange—hence the subscript "OGE." On the other hand, $\mathrm{BD}_{\mathrm{CI}}$ is diagonal in color and color independent—hence the subscript "CI." $\mathrm{BD}_{\mathrm{OGE}}$ and $\mathrm{BD}_{\mathrm{CI}}$ have three terms each that describe pairwise interactions in quark-quark, quark-antiquark, and antiquark-antiquark pairs. The factor $1/2$ that multiplies quark-quark as well as antiquark-antiquark terms is present because the two quarks, or the two antiquarks, that interact are indistinguishable. Finally, a is a constant between 0 and 1, and $C_F = (N_c^2 - 1)/(2N_c) = 4/3$ is the value of the quadratic Casimir operator in a fundamental representation of $SU(N_c)$, $N_c = 3$. We choose $a = 0.85$; therefore, in our Hamiltonian 85% of longitudinal confining strength in a meson comes from the OGE-like term, and 15% comes from the color-independent term. See below for a more detailed discussion.

The kernels are

$$U_{\mathrm{conf},\perp} = \kappa^4 \delta_{\sigma_1,\sigma_{1'}} \delta_{\sigma_2,\sigma_{2'}} 4\pi \delta(x_{12} - x_{1'2'}) (x_{12} x_{21})^2 \times \left[\frac{\partial^2}{\partial \mathbf{k}_{1'2'}^2} (2\pi)^2 \delta^2(\mathbf{k}_{1'2'} - \mathbf{k}_{12}) \right], \tag{14}$$

$$U_{\mathrm{conf},z} = \kappa^4 \delta_{\sigma_1,\sigma_{1'}} \delta_{\sigma_2,\sigma_{2'}} (2\pi)^2 \delta^2(\mathbf{q}_{12} - \mathbf{q}_{1'2'}) \times \left[-\frac{1}{\sqrt{D_{12}}} \frac{\partial}{\partial x_{12}} \frac{1}{\sqrt{D_{12}}} \frac{1}{\sqrt{D_{1'2'}}} \frac{\partial}{\partial x_{1'2'}} \frac{1}{\sqrt{D_{1'2'}}} \times 4\pi \delta(x_{1'2'} - x_{12}) \right], \tag{15}$$

where κ is the interaction strength parameter, $x_{12} = p_1^+/(p_1^+ + p_2^+)$ is the longitudinal momentum fraction of particle 1 with respect to 2, and $x_{21} = 1 - x_{12}$ is the longitudinal momentum fraction of particle 2 with respect to particle 1. The relative transverse momentum is $\mathbf{k}_{12} = x_{21}\mathbf{p}_1 - x_{12}\mathbf{p}_2$. Moreover,

$$\mathbf{q}_{12} = \frac{\mathbf{k}_{12}}{\sqrt{x_{12} x_{21}}}, \tag{16}$$

$$q_{12}^z = m \frac{x_{12} - x_{21}}{\sqrt{x_{12} x_{21}}}, \tag{17}$$

and

$$D_{12} = \frac{dq_{12}^z}{dx_{12}}(x_{12}) = \frac{m}{2[x_{12}(1 - x_{12})]^{3/2}}. \tag{18}$$

Objects with the subscript $1'2'$ are defined in the same way as objects with the subscript 12, except that 1 is replaced by $1'$ and 2 is replaced by $2'$.

The confining potential is determined by the anti–de Sitter (AdS)/QCD holography [65], and its transverse part reproduces the AdS/QCD harmonic oscillator in the $Q\bar{Q}$ sector. With appropriate momentum variables [66], in the $Q\bar{Q}$ sector, the longitudinal and transverse terms complement each other and form a three-dimensional, rotationally invariant harmonic oscillator; see Eq. (26). The potentials in the $Q\bar{Q}$ sector are naturally extended to other sectors through Eqs. (9) and (10), which act in all sectors. The extension, however, is not unique. For example, the factor $p_1^+ + p_2^+$ could be replaced by the total P^+. Moreover, $\mathrm{BD}_{\mathrm{OGE}}$ and $\mathrm{BD}_{\mathrm{CI}}$ evaluate to the same expression between states in the $Q\bar{Q}$ sector up to a factor of C_F. Their combination, as in Eq. (10), gives a result that is independent of a in the $Q\bar{Q}$ sector. Our choice of the confining potential was obtained after studying several variants and searching for the acceptable spectral behavior of the solutions.

We found that removing the color-independent part or replacing $p_1^+ + p_2^+$ with P^+ leads to the appearance of unphysical solutions with negative mass squared. While in general tachyonlike states can be a sign of unstable equilibrium in a linear approximation of a field theory (see Ref. [67]), our approach is nonperturbative and we are dealing with model Hamiltonians. Therefore, we regard candidate model Hamiltonians with such tachyonic solutions as unphysical. The properties of these states are very far from the properties expected of bound tetraquark states. For example, the dominant components of wave functions of these nonphysical states reveal a very fast motion of quarks with respect to each other, making them more like highly excited, high momentum scale states than like states characterized by the low relative momenta appropriate for our model. $a = 0.85$ is the largest value of a that guarantees that no negative M^2 states will appear up to $K = 50$ for $N_{\max} = 6$ (see Sec. III). It is worth noting that exchange potentials consisting of two or more gluons are in general mixtures of OGE-like and color-independent parts. Hence, our confining potential appears to be reasonable, apart from the fact that our CI potential confines at large distances. However, the states which should be affected the most by this confinement are the excited states, while we focus mainly on the ground state.

The Hamiltonian term of the one-gluon-exchange interaction is $H_{\mathrm{OGE}} = P^+ V_{\mathrm{OGE}}$, where

$$V_{\mathrm{OGE}} = \int_{121'2'} \tilde{\delta}_{12.1'2'} U_{\mathrm{OGE}}(1,2;1',2') \mathrm{BD}_{\mathrm{OGE}}. \tag{19}$$

The kernel of the OGE term is

$$U_{\mathrm{OGE}}(1,2;1',2') = -g^2 \frac{\bar{u}_1 \gamma_\mu u_{1'} \bar{u}_2 \gamma^\mu u_{2'}}{(x_{12} - x_{1'2'})\mathcal{D}} \sqrt{p_1^+ p_2^+ p_{1'}^+ p_{2'}^+}, \tag{20}$$

where $\mathcal{D}$ is the energy denominator,

$$\mathcal{D} = \frac{1}{2}\left[\frac{\mathbf{p}_1^2+m^2}{x_{12}} - \frac{\mathbf{p}_{1'}^2+m^2}{x_{1'2'}} - \frac{\mathbf{p}_2^2+m^2}{x_{21}} + \frac{\mathbf{p}_{2'}^2+m^2}{x_{2'1'}}\right] - \frac{(\mathbf{p}_1-\mathbf{p}_{1'})^2+\mu^2}{x_{12}-x_{1'2'}}, \tag{21}$$

with μ being a fictitious gluon mass. We use the same spinors as those in Ref. [55], and $\bar{u}_1\gamma_\mu u_{1'}\bar{u}_2\gamma^\mu u_{2'}$ can be found in Table I therein. The fictitious gluon mass μ is introduced to regulate the Coulomb singularity: if we take $\mathbf{p}_1 = \mathbf{p}_{1'}$ and $x_{12} = x_{1'2'}$, then $(x_{12}-x_{1'2'})\mathcal{D}$, which is in the denominator of Eq. (20), becomes zero unless $\mu \neq 0$. This singularity is integrable if the momenta are continuous; however, in BLFQ we discretize the longitudinal momenta and the singularity somehow has to be regulated. Even though diagonal matrix elements of the discretized version of H_{OGE} diverge as $\mu \to 0$, the eigenvalues and eigenvectors approach a finite limit.

The Hamiltonian of Eq. (3) provides a unified description of the $Q\bar{Q}$ and $QQ\bar{Q}\,\bar{Q}$ systems. In fact, one could apply this Hamiltonian in sectors with an arbitrary number of heavy quarks and antiquarks. We use it in three separate calculations for three purposes. In all three cases we restrict the space of states to color singlets, which can be achieved since H conserves color. Details are provided in the Appendix. First, we solve the $Q\bar{Q}$ eigenvalue problem and, by fitting the numerical spectrum to the experimental spectrum of charmonium, we fix the free parameters of the Hamiltonian: quark mass m, confining potential strength parameter κ and OGE coupling constant g. Second, we solve the $QQ\bar{Q}\,\bar{Q}$ eigenvalue problem to find the four-quark ground-state mass. Third, we solve the $QQ\bar{Q}\,\bar{Q}$ eigenvalue problem with some interactions turned off. The interactions that are kept allow one quark to form a meson with one antiquark, and the other quark to form a meson with the other antiquark. There is no interaction between the two mesons, and we restrict the space of states to the states in which both mesons are color singlets separately. This way we can numerically estimate the two-meson threshold, which can be different than the sum of the masses of two mesons obtained in the $Q\bar{Q}$ calculation due to the finite basis. Below we briefly present the three cases.

C. Eigenvalue equation for mesons

The Hamiltonian can have many eigenvectors of various forms. States that describe a single meson with fixed momenta P_M^+ and $\mathbf{P}_M$ are of the form

$$|\psi_M\rangle = \int_{12} P_M^+ \tilde{\delta}_{12.P_M}\psi_M(12) b_1^\dagger d_2^\dagger|0\rangle. \tag{22}$$

The "front form energy" of the meson is $P_M^- = \frac{M^2+\mathbf{P}_M^2}{P_M^+}$, where M is the mass of the meson. P_M^μ are eigenvalues of operators P^μ, and M^2 is an eigenvalue of H. The eigenvalue equation $H|\psi_M\rangle = M^2|\psi_M\rangle$ reduces to

$$\frac{m^2+\mathbf{k}_{12}^2}{x_1}\psi_M(12) + \frac{m^2+\mathbf{k}_{12}^2}{x_2}\psi_M(12) + \sum_{c_{1'},c_{2'}}\kappa^4\tilde{U}_{12}\psi_{Mc_{1'}c_{2'}}(12) - \int_{1'2'} P_M^+\tilde{\delta}_{1'2'.P_M}t^a_{11'}t^a_{2'2} \times U_{\mathrm{OGE}}(1,2;1',2')\psi_M(1'2') = M^2\psi_M(12), \tag{23}$$

where

$$\tilde{U}_{12} = t^a_{11'}t^a_{2'2}x_{12}x_{21}(\mathbf{r}_1-\mathbf{r}_2)^2 - \left[at^a_{11'}t^a_{2'2} + \frac{4}{3}(1-a)\delta_{c_1,c_{1'}}\delta_{c_2,c_{2'}}\right] \times \frac{1}{\sqrt{D_{12}}}\frac{\partial}{\partial x_{12}}\frac{1}{D_{12}}\frac{\partial}{\partial x_{12}}\frac{1}{\sqrt{D_{12}}}. \tag{24}$$

One can simplify the form of this equation considerably by changing the variables from $\mathbf{k}_{12}$ and x_{12} to $\mathbf{q}_{12}$ and q_{12}^z (collectively denoted as $\vec{q}_{12}$), which were introduced in Eqs. (16) and (17). Moreover, we assume that the meson is a color-singlet state. Therefore,

$$\psi_M(12) = \frac{\delta_{c_1,c_2}}{\sqrt{N_c}}\sqrt{D_{12}}\phi_{\sigma_1\sigma_2}(\vec{q}_{12}). \tag{25}$$

We get

$$(4m^2+\vec{q}_{12}^2)\phi_{\sigma_1\sigma_2}(\vec{q}_{12}) - C_F\kappa^4\frac{\partial^2}{\partial\vec{q}_{12}^2}\phi_{\sigma_1\sigma_2}(\vec{q}_{12}) - C_F\sum_{\sigma_{1'},\sigma_{2'}}\int\frac{d^3q_{1'2'}}{(2\pi)^3}\frac{U_{\mathrm{OGE}}(1,2;1',2')}{2\sqrt{D_{12}D_{1'2'}}}\phi_{\sigma_{1'}\sigma_{2'}}(\vec{q}_{1'2'}) = M^2\phi_{\sigma_1\sigma_2}(\vec{q}_{12}). \tag{26}$$

This equation looks much like a nonrelativistic Schrödinger equation in momentum space. The Laplacian acting on the wave function is equivalent to a rotationally symmetric harmonic-oscillator potential, and the OGE potential is written in a generic form. It is worth noting that the same confining potential can be derived using RGPEP with a gluon mass ansatz [68,69]. Our OGE potential differs from the Coulomb plus Breit-Fermi equation in Ref. [68] and is taken instead from Ref. [55]. The choice was dictated by the availability of software implementation of the latter potential. Similarly, instead of the longitudinal potential given in Eq. (15) we could have chosen a kernel that would give us the $\partial_x x(1-x)\partial_x$ potential of Refs. [45,46]. In the limit of relative momenta vanishing with respect to the quark masses the two potentials become equal; hence, both should be suitable for phenomenology. It is sufficient for

our purposes to select one longitudinal confining potential and one OGE potential and work with them.

D. Eigenvalue equation for tetraquarks

Tetraquark states have a form very similar to that of meson states,

$$|\psi_T\rangle = \int_{1234} P_T^+ \tilde{\delta}_{1234.P_T} \psi_T(1234) b_1^\dagger b_2^\dagger d_3^\dagger d_4^\dagger |0\rangle. \quad (27)$$

This state has the fixed momenta P_T^+ and $\mathbf{P}_T$, while $P_T^- = \frac{M^2+\mathbf{P}_T^2}{P_T^+}$. The eigenvalue equation $H|\psi_T\rangle = M^2|\psi_T\rangle$ reduces to

$$\sum_{i=1}^{4} \frac{m^2+\mathbf{k}_i^2}{x_i}\psi_T(1234) + \sum_{i<j}\kappa^4 \tilde{U}_{ij}\psi_T(1234) + \sum_{i<j}\frac{1}{x_i+x_j}\int_{i'j'}(p_i^+ + p_j^+)\tilde{\delta}_{ij.i'j'}W_{\mathrm{OGE}}(i,j;i',j')\psi' = M^2\psi_T(1234), \quad (28)$$

where $x_i = p_i^+/P_T^+$ and $\sum_{i=1}^4 x_i = 1$, while $\mathbf{k}_i$ is a transverse momentum of particle i in a rest frame of the bound state where $\sum_{i=1}^4 \mathbf{k}_i = 0$. The harmonic oscillator $\tilde{U}_{ij}$ for the quark-antiquark interaction is given in Eq. (24), with 1, 2, 1′, and 2′ replaced by i, j, i', and j', respectively. For quark-quark and antiquark-antiquark interactions it is

$$\tilde{U}_{ij} = -t_{ii'}^a t_{jj'}^a x_{ij}x_{ji}(\mathbf{r}_i-\mathbf{r}_j)^2 + \left[a t_{ii'}^a t_{jj'}^a - \frac{4}{3}(1-a)\delta_{c_i,c_{i'}}\delta_{c_j,c_{j'}}\right] \times \frac{1}{\sqrt{D_{ij}}}\frac{\partial}{\partial x_{ij}}\frac{1}{D_{ij}}\frac{\partial}{\partial x_{ij}}\frac{1}{\sqrt{D_{ij}}}. \quad (29)$$

$W_{\mathrm{OGE}}(i,j;i',j')\psi'$ differs depending on i and j. For the quark-quark interaction, i.e., $i=1$ and $j=2$,

$$W_{\mathrm{OGE}}(1,2;1',2')\psi' = \frac{t_{11'}^a t_{22'}^a U_{\mathrm{OGE}}(1,2;1',2') - t_{12'}^a t_{21'}^a U_{\mathrm{OGE}}(1,2;2',1')}{2} \times \psi_T(1'2'34). \quad (30)$$

For the antiquark-antiquark interaction, $i=3$ and $j=4$,

$$W_{\mathrm{OGE}}(3,4;3',4')\psi' = \frac{t_{3'3}^a t_{4'4}^a U_{\mathrm{OGE}}(3,4;3',4') - t_{4'3}^a t_{3'4}^a U_{\mathrm{OGE}}(3,4;4',3')}{2} \times \psi_T(123'4'). \quad (31)$$

For quark-antiquark interactions, $i=1$ or 2 and $j=3$ or 4,

$$W_{\mathrm{OGE}}(i,j;i',j')\psi' = -t_{ii'}^a t_{j'j}^a U_{\mathrm{OGE}}(i,j;i',j')\psi_{i'j'}, \quad (32)$$

where $\psi_{i'j'} = \psi_T(1'23'4)$, $\psi_T(1'234')$, $\psi_T(12'3'4)$, and $\psi_T(12'34')$ for $ij = 13$, 14, 23, and 24, respectively. The interaction kernels are antisymmetrized as a result of having the identical particles $b_1^\dagger b_2^\dagger$ and $d_3^\dagger d_4^\dagger$ in Eq. (27).

E. Eigenvalue equation for two mesons

To describe two separate mesons A and B, we choose

$$|\psi_{AB}\rangle = \int_{13} P_A^+ \tilde{\delta}_{13.P_A}\psi_A(13) b_1^\dagger d_3^\dagger \times \int_{24} P_B^+ \tilde{\delta}_{24.P_B}\psi_B(24) b_2^\dagger d_4^\dagger |0\rangle. \quad (33)$$

Meson A has the momentum components P_A^+ and $\mathbf{P}_A$, while meson B has the momentum components P_B^+ and $\mathbf{P}_B$. By placing the two mesons far enough from each other, we can make the total interaction between them arbitrarily small. We simulate this situation by turning off all interactions except those between particles 1 and 3, which form meson A, and between particles 2 and 4, which form meson B. Moreover, two identical quarks contained in two separated mesons are in practice distinguishable. Therefore, in this section we treat all particles as distinguishable. Since there are no interactions between the two mesons, we expect that in the general eigenvalue equation,

$$H|\psi_{AB}\rangle = M^2|\psi_{AB}\rangle, \quad (34)$$

the eigenvalue M^2 can be written as the invariant mass of two mesons with masses M_A and M_B,

$$M^2 = (P_{A\mu}+P_{B\mu})(P_A^\mu + P_B^\mu) = \frac{M_A^2+\mathbf{k}_{AB}^2}{x_A} + \frac{M_B^2+\mathbf{k}_{AB}^2}{x_B}. \quad (35)$$

The relative transverse momentum between mesons is $\mathbf{k}_{AB} = x_B\mathbf{P}_A - x_A\mathbf{P}_B$, where $x_A = P_A^+/(P_A^+ + P_B^+) = x_1 + x_3$, $x_B = x_2 + x_4$. Equation (34) reduces to

$$\frac{1}{x_A}\mathcal{E}_A\psi_B(24) + \frac{1}{x_B}\mathcal{E}_B\psi_A(13) = \left(\frac{M_A^2}{x_A}+\frac{M_B^2}{x_B}\right)\psi_A(13)\psi_B(24), \quad (36)$$

where

$$\mathcal{E}_A = \frac{m^2+\mathbf{k}_{13}^2}{x_{13}x_{31}}\psi_A(13) - x_A\sum_{c_{1'},c_{3'}}\kappa^4\tilde{U}_{13}\psi_{Ac_{1'}c_{3'}}(13) - \int_{1'3'} P_A^+\tilde{\delta}_{1'3'.P_A}t_{11'}^a t_{3'3}^a U_{\mathrm{OGE}}(1,3;1',3')\psi_A(1'3'), \quad (37)$$

$$\mathcal{E}_B = \frac{m^2+\mathbf{k}_{24}^2}{x_{24}x_{42}}\psi_B(24) - x_B\sum_{c_{2'},c_{4'}}\kappa^4\tilde{U}_{24}\psi_{Bc_{2'}c_{4'}}(24) - \int_{2'4'} P_B^+\tilde{\delta}_{2'4'.P_B}t^a_{22'}t^a_{4'4}U_{\rm OGE}(2,4;2',4')\psi_B(2'4'). \tag{38}$$

Note that the relative transverse kinetic energy between the mesons in the eigenvalue, $\mathbf{k}_{AB}^2/x_A + \mathbf{k}_{AB}^2/x_B$, canceled with the transverse kinetic energy between mesons in $H_{\rm kinetic}$, which is fixed by the choice of state $|\psi_{AB}\rangle$. We separate Eq. (36) in two, $\mathcal{E}_A = M_A^2\psi_A(13)$ and $\mathcal{E}_B = M_B^2\psi_B(24)$. Using the same kind of substitution as in Sec. II C,

$$\psi_A(13) = \frac{\delta_{c_1,c_3}}{\sqrt{N_c}}\sqrt{D_{13}}\phi_{A\sigma_1\sigma_3}(\vec{q}_{13}), \tag{39}$$

$$\psi_B(24) = \frac{\delta_{c_2,c_4}}{\sqrt{N_c}}\sqrt{D_{24}}\phi_{B\sigma_2\sigma_4}(\vec{q}_{24}), \tag{40}$$

we get two eigenvalue equations,

$$(4m^2+\vec{q}_{13}^2)\phi_{A\sigma_1\sigma_3}(\vec{q}_{13}) - x_AC_F\kappa^4\frac{\partial^2}{\partial\vec{q}_{13}^2}\phi_{A\sigma_1\sigma_3}(\vec{q}_{13}) - C_F\sum_{\sigma_{1'},\sigma_{3'}}\int\frac{d^3q_{1'3'}}{(2\pi)^3}\frac{U_{\rm OGE}(1,3;1',3')}{2\sqrt{D_{13}D_{1'3'}}} \times\phi_{A\sigma_{1'}\sigma_{3'}}(\vec{q}_{1'3'}) = M_A^2\phi_{A\sigma_1\sigma_3}(\vec{q}_{13}), \tag{41}$$

$$(4m^2+\vec{q}_{24}^2)\phi_{B\sigma_2\sigma_4}(\vec{q}_{24}) - x_BC_F\kappa^4\frac{\partial^2}{\partial\vec{q}_{24}^2}\phi_{B\sigma_2\sigma_4}(\vec{q}_{24}) - C_F\sum_{\sigma_{2'},\sigma_{4'}}\int\frac{d^3q_{2'4'}}{(2\pi)^3}\frac{U_{\rm OGE}(2,4;2',4')}{2\sqrt{D_{24}D_{2'4'}}} \times\phi_{B\sigma_{2'}\sigma_{4'}}(\vec{q}_{2'4'}) = M_B^2\phi_{B\sigma_2\sigma_4}(\vec{q}_{24}). \tag{42}$$

F. Cluster decomposition principle

The two-meson solutions in the $QQ\bar{Q}\,\bar{Q}$ sector provide a good example of how the cluster decomposition principle works in the front form of Hamiltonian dynamics. There are several elements needed for the cluster decomposition principle to be satisfied. First, the mass M_A of meson A should not depend on the state of particles in meson B. Similarly, the mass M_B of meson B should not depend on the state of the particles in meson A. Second, M_A and M_B calculated in the $QQ\bar{Q}\,\bar{Q}$ sector should be equal to the corresponding masses in the $Q\bar{Q}$ sector. For example, if meson A is in the 0^{-+} ground state and meson B is in the 1^{--} ground state, then M_A should be exactly equal to the mass of η_c calculated in the $Q\bar{Q}$ sector and M_B should be exactly equal to the mass of J/ψ calculated in the $Q\bar{Q}$ sector. This is expected from the analytic solutions; numerical solutions may differ slightly.

In the two-meson example in Sec. II E, those conditions are not satisfied. Comparing Eqs. (41) and (26), one can see that in Eq. (41) there is an extra factor x_A multiplying the confining potential. Since x_A is fixed, the mass M_A is independent of whether meson B is in the η_c or J/ψ or any other state. Nevertheless, M_A depends on P_B^+ because x_A depends on P_B^+. Moreover, M_A cannot be the same as the mass of the corresponding charmonium in the $Q\bar{Q}$ sector, because the strength of the confining potential in the $Q\bar{Q}$ sector is $C_F\kappa^4$, while it is $x_AC_F\kappa^4$ for meson A in the $QQ\bar{Q}\,\bar{Q}$ sector.

We could formally restore the decomposition principle by replacing $p_1^+ + p_2^+$ in Eqs. (9) and (10) with P^+, but this would lead to the appearance of spurious states, as described in Sec. II B. We prioritize the acceptable spectrum over exact conservation of the decomposition principle since the former is more important in practice, while the latter can be approximately restored. Since charm quarks are heavy, the two-meson system and tetraquark can be considered nonrelativistic. Therefore, $x_A \approx x_B \approx 1/2$, and one can partly restore the cluster decomposition principle by rescaling κ in the $QQ\bar{Q}\,\bar{Q}$ sector. In other words, in the $QQ\bar{Q}\,\bar{Q}$ sector we use $\kappa_T = 2^{1/4}\kappa$ instead of κ. This guarantees that $x_AC_F\kappa_T^4 \approx C_F\kappa^4$ for $x_A \approx 1/2$.

As opposed to the confining potential, the OGE potential fully obeys the cluster decomposition principle. This is to be expected because it can be derived from QCD in perturbation theory. In fact, all two-body potentials in QCD have the same generic form of Eq. (19) (apart from the color factors, which may differ). It is important for $U_{\rm OGE}(1,2;1',2')$ to depend only on the relative momenta between particles 1 and 2 and between $1'$ and $2'$, and not on, e.g., the momentum fractions x_1 or x_2, which depend on the total P^+ of the system. Therefore, Eq. (19) illustrates the general form of two-body operators that admit the cluster decomposition principle in the sense described here. A more general treatment of relativistic theories obeying cluster separability can be found in Ref. [70].

In the eigenvalue equations the cluster decomposition principle manifests itself through the presence of the $1/x_A$ and $1/x_B$ factors in Eq. (36) and the $1/(x_i+x_j)$ factor in Eq. (28) that multiply interaction terms that depend only on relative momenta within the interacting pair, with no trace of the total P^+. Note that momentum conservation in $\int_{i'j'}(p_i^+ + p_j^+)\tilde{\delta}_{ij.i'j'}$ fixes $p_{i'} + p_{j'}$, and one is left with an integral over the relative momenta $x_{i'j'}$ and $\mathbf{k}_{i'j'}$.

III. BASIS LIGHT-FRONT QUANTIZATION AND TRUNCATION SCHEME

Basis light-front quantization is a basis function approach to Hamiltonian light-front field theories [42]. Longitudinal and transverse directions are treated differently. In the

longitudinal direction a box of length $2L$, i.e., coordinate $x^- \in [-L, L]$, is introduced. This leads to discretization of the longitudinal momenta. We apply antiperiodic boundary condition for the quark field, which means that quark longitudinal momenta can take only the values

$$p^+ = \frac{2\pi}{L} k, \tag{43}$$

where k is called the longitudinal quantum number and it is a positive half integer. In sectors with many particles, the total longitudinal momentum is by definition $P^+ = \frac{2\pi}{L} K$, where $K = \sum_i k_i$ is the sum of longitudinal quantum numbers of all particles. In Sec. II P^+ denoted the momentum operator; from now on, P^+ indicates the eigenvalue of the operator P^+ and we keep it fixed (we use only eigenstates of the operator P^+ with eigenvalue P^+). For a given particle i, the longitudinal momentum fraction x_i is

$$x_i = \frac{p_i^+}{P^+} = \frac{k_i}{K}. \tag{44}$$

The longitudinal continuum limit is $L, K \to \infty$, while P^+ is kept fixed. None of the quantities that we calculate depend on the exact values of P^+ and L due to front form boost invariance.

For transverse momenta we introduce the harmonic-oscillator basis [42]. We define the new creation and annihilation operators as

$$B_i = \frac{1}{\sqrt{P^+}} \int \frac{d^2q}{(2\pi)^2} \Psi_{n_i}^{m_i}(\mathbf{q})^* b_i|_{\mathbf{p}_i = \sqrt{x_i}\mathbf{q}}, \tag{45}$$

$$D_i = \frac{1}{\sqrt{P^+}} \int \frac{d^2q}{(2\pi)^2} \Psi_{n_i}^{m_i}(\mathbf{q})^* d_i|_{\mathbf{p}_i = \sqrt{x_i}\mathbf{q}}. \tag{46}$$

Note that the operators B_i and D_i depend on the discrete quantum numbers n_i, m_i, k_i, σ_i, and c_i, while the plane-wave operators b_i and d_i depend on the continuum transverse momentum $\mathbf{p}_i = \sqrt{x_i}\mathbf{q}$, the discretized longitudinal momentum $p_i^+ = 2\pi k_i / L$ (or, equivalently, on k_i), and the spin and color σ_i and c_i. Operators B_i and D_i are normalized to unity, that is,

$$\{B_i, B_j^\dagger\} = \{D_i, D_j^\dagger\} = \delta_{n_i,n_j}\delta_{m_i,m_j}\delta_{k_i,k_j}\delta_{\sigma_i,\sigma_j}\delta_{c_i,c_j}. \tag{47}$$

The basis wave functions are

$$\Psi_n^m(\mathbf{q}) = \frac{1}{b}\sqrt{\frac{4\pi n!}{(n+|m|)!}} L_n^{|m|}\left(\frac{q^2}{b^2}\right) e^{-\frac{q^2}{2b^2}} \left|\frac{q}{b}\right|^{|m|} e^{im\varphi}, \tag{48}$$

where $L_n^{|m|}$ are the associated Laguerre polynomials, $q = \sqrt{(q^1)^2 + (q^2)^2}$, $\varphi = \arg \mathbf{q}$, and b is a selectable positive parameter of dimension of $\mathbf{P}$. The principal quantum number n is a non-negative integer, while m can be an arbitrary integer. The choice of the harmonic-oscillator wave functions is compatible with our choice of the transverse confining potential and is important for the factorization of the center-of-mass motion, which we describe in detail later in this section.

In practice one has to truncate the many-particle basis in the transverse direction by limiting the allowed radial numbers n_i and angular numbers m_i to a cutoff in the number of oscillator quanta in each basis state,

$$\sum_i (2n_i + |m_i| + 1) \le N_{\max}. \tag{49}$$

Removing this truncation is equivalent to taking the limit $N_{\max} \to \infty$. In addition, we require our multiparticle basis state to have the total angular momentum projection

$$M_J = \sum_i (m_i + \sigma_i), \tag{50}$$

where $\sigma_i = \pm\frac{1}{2}$ is the fermion light-front helicity. Throughout this article we limit our attention to $M_J = 0$ states.[1] It is also worth mentioning that the truncation of the basis breaks the cluster decomposition principle. For example, if we consider our two-meson example from Sec. II E and if the quantum numbers of particles forming meson A already almost saturate Eq. (49), then the particles of meson B will be restricted to a much smaller space of states than the particles of meson A. The opposite situation is also possible and is included in the truncated basis. Therefore, one meson can influence the other through the truncation, even if there are no interactions between them. Moreover, each of the mesons in the $Q\bar{Q}Q\bar{Q}$ sector is subject to a different truncation than the one meson in the $Q\bar{Q}$ sector and meson masses in the $Q\bar{Q}$ and $Q\bar{Q}Q\bar{Q}$ sectors can differ slightly, but the difference should vanish as the basis size is increased.

It is straightforward to rewrite the Hamiltonian presented in Sec. II using new operators B and D. One has to additionally discretize the longitudinal momenta by following a simple prescription, $4\pi\delta(p_1^+ - p_2^+) \to 2L\delta_{k_1,k_2}$, $\int_0^\infty \frac{dp^+}{4\pi} \to \frac{1}{2L}\sum_k$, $b \to \sqrt{2L}b$, $d \to \sqrt{2L}d$. Then it is only a matter of computing the matrix elements of H and diagonalizing the obtained matrix to obtain the eigenstates of H and their masses. Computation of matrix elements between states containing two quarks and two antiquarks is not much more complicated than the analogous computation between

[1] A tetraquark state with $M_J = 0$ can, in principle, be built from one meson having, for example, $M_J = +1$, and the other having $M_J = -1$. However, this is not expected to play a role in calculations focused on the tetraquark ground state since such states would be expected to result in a higher tetraquark dissociation threshold than the one where both mesons have $M_J = 0$.

states containing only one quark and one antiquark, because no particle or any pair of particles is distinguished. One obviously has to calculate terms for all six pairs of particles instead of just one, and interactions between identical particles must be property antisymmetrized. Using a basis in relative momenta of the Jacobi type, for example, would require us to use different formulas for different pairs of interacting particles. It should be evident that the addition of more particles to our calculation (including gluons) would be straightforward. Admittedly, this comes at the cost of larger matrices (effectively one more particle per Fock sector compared to Jacobi coordinates), but the larger matrices are also more sparse, which aids applications on modern computers, while the simplicity makes the software development more reliable. Probably the most important complication is introduced by restricting our space of states to only color-singlet states. This important, but rather technical, topic is described in more detail in the Appendix. Similar basis spaces restricted to include only color singlets have been implemented for a BLFQ treatment of glueballs with Fock spaces having up to six gluons [71].

Since BLFQ implements states using single-particle transverse motion instead of relative motion, the resulting eigenvectors will possess center-of-mass motion excitations which are of no interest to us because they do not influence the invariant mass or the internal structure of hadrons on the light front. The harmonic-oscillator basis allows us to easily deal with this problem. By adopting Eq. (49) the eigenvectors of the truncated Hamiltonian have a known and simple center-of-mass motion. This can be demonstrated by showing that, even in the truncated basis, H commutes with the similarly truncated center-of-mass harmonic-oscillator Hamiltonian

$$H_{\mathrm{CM}} = \lambda_{\mathrm{CM}}(\mathbf{P}^2 + b^4\mathbf{R}^2 - 2b^2), \tag{51}$$

where $\mathbf{P}$ is the transverse momentum operator and $\mathbf{R}$ is the transverse center-of-mass position operator,

$$\mathbf{R} = \sum_{k_1,k_2,\sigma_1,\sigma_2,c_1,c_2} \frac{\delta_{k_1,k_2}\delta_{\sigma_1,\sigma_2}\delta_{c_1,c_2}}{P^+} \int \frac{d^2\mathbf{p}_1}{(2\pi)^2} \int \frac{d^2\mathbf{p}_2}{(2\pi)^2} \times \left[-i\frac{\partial}{\partial \mathbf{p}_1}(2\pi)^2\delta^2(\mathbf{p}_1 - \mathbf{p}_2)\right](b_1^\dagger b_2 + d_1^\dagger d_2). \tag{52}$$

Eigenvalues of H_{CM} are $n \cdot 2b^2\lambda_{\mathrm{CM}}$, where n is a nonnegative integer. $n = 0$ corresponds to the ground state of center-of-mass motion and $n \geq 1$ correspond to excited states of the center-of-mass motion. In a typical scenario among eigenstates of H with the lowest eigenvalues, there will be states with the same relative motion but a different center-of-mass motion. To keep only the eigenstates with the ground-state center-of-mass motion, we diagonalize $H + H_{\mathrm{CM}}$ instead of H. Since H and H_{CM} commute, they have the same eigenvectors, while the eigenvalues of the sum will be the sum of the eigenvalues of H and H_{CM}. Therefore, states with an excited-state center-of-mass motion will be shifted up by a multiple of $2b^2\lambda_{\mathrm{CM}}$. Choosing λ_{CM} sufficiently large and positive, all states with an excited center-of-mass motion will have eigenvalues larger than the eigenvalues of the limited number of states that we obtain numerically. We use $\lambda_{\mathrm{CM}} = 50$ in our calculations.

IV. ANALYSIS OF BINDING ENERGY

To address the question of whether there are $cc\bar{c}\,\bar{c}$ states that cannot break up into two charmonia, we need to know the mass of the lowest tetraquark state and the value of the two-charmonium threshold taking into account the implications of the truncated basis space for the subsystems. We obtain estimates of both by numerically diagonalizing the truncated matrices of our model Hamiltonian obtained using BLFQ. We therefore solve three problems which correspond to three eigenvalue equations presented in Secs. II C–II E. The discrete spectra of truncated Hamiltonians should look more and more like the spectrum of the untruncated, infinite Hamiltonian as $N_{\mathrm{max}} \to \infty$ and $K \to \infty$.

The Hamiltonian matrix in the sector with one meson is used to fix the free parameters of the model, m, κ, and $\alpha = g^2/(4\pi)$. The gluon mass $\mu = 10$ MeV and the basis parameter b in the meson calculation is fixed to be equal to κ. We fit the lowest eight states in the spectrum of charmonium. The root mean square difference between the fitted and experimental masses is 31 MeV. The parameters are given in Table I, while Table II lists the fitted meson masses and the corresponding experimental values. The fitting was carried out for $N_{\mathrm{max}} = 6$ and $K = 9$. In all calculations we calculate $M_J = 0$ states. For the purpose of estimating the two-meson threshold [see Eq. (55)], we also calculated meson masses for all $2 \leq N_{\mathrm{max}} \leq 10$ and $1 \leq K \leq 17$, and $c\bar{c}$ masses with interactions between c and $\bar{c}$ turned off for the same range of N_{max} and K. The lowest possible N_{max} in a system with two particles is 2, while the lowest K is 1. The upper bounds on N_{max} and K for a meson

TABLE I. Parameters obtained from a fit to an experimental meson spectrum.

m	κ	α
1.25 GeV	1.21 GeV	0.367

TABLE II. Fitted masses in MeV. $N_{\mathrm{max}} = 6$, $K = 9$.

	$\eta_c(1S)$	J/ψ	χ_{c0}	χ_{c1}	χ_{c2}	h_c	$\eta_c(2S)$	$\psi(2S)$
Fit	3031	3067	3415	3517	3564	3474	3676	3666
Expt.	2984	3097	3415	3511	3556	3525	3637	3686

are determined by the largest $N_{\max}$ and K that we used in the tetraquark computations.

Tetraquark masses are calculated for $N_{\max} = 6, 8, 10, 12$ and for $K = 6, 10, 14, 18$. We calculated three sets of tetraquark masses: masses with all interactions turned on [cf. Eq. (28)], masses with all interactions turned off, $\kappa = 0$, $\alpha = 0$, and masses with only interactions in the pair 13 and in the pair 24 turned on [cf. Eq. (36)]. For the purpose of the tetraquark calculations, we readjust the parameter b to remove a possible source of mismatch between meson and tetraquark calculations. The characteristic value of q in Eq. (48) is b, which means that the characteristic value of $|\mathbf{p}|$ is $\sqrt{x}b$. In the tetraquark case, similarly, we have $|\mathbf{p}| \sim \sqrt{x}b$. However, in the meson case, the expected value of x is $1/2$, while in the tetraquark case the expected value of x is $1/4$. Therefore, it is reasonable to take $b_T = \sqrt{2}b_M$, where b_T is the value of b for tetraquark calculations and b_M is the value of b for meson calculations. This way the characteristic scale of $|\mathbf{p}|$ in the basis is the same in the two cases. This readjustment is not strictly necessary, because for sufficiently large $N_{\max}$ and K the results should be rather insensitive to the choice of b for fixed κ over a wide range of values of b, but it should increase the utility of the results for small $N_{\max}$ and K. Moreover, as mentioned in Sec. II F, instead of κ we use $\kappa_T = 2^{1/4}\kappa$ for the confining strength parameter.

One of the sources of systematic errors of the framework that we adopt originates from the fact that a pair of particles in a $cc\bar{c}\,\bar{c}$ system has a minimal nonzero kinetic energy with respect to the other two particles. The minimal kinetic energy should approach zero from above as $N_{\max}$ approaches infinity, but it may be of importance for finite $N_{\max}$. This artifact of a finite basis is called "kinetic energy penalty" in Ref. [6]. Here we estimate it in the following way,

$$\Delta M^2 = M^{2\,\mathrm{free}}_{cc\bar{c}\,\bar{c}}(N_{\max}, K) - \min_{N_1,K_1}\left[\frac{M^{2\,\mathrm{free}}_{c\bar{c}}(N_1,K_1)}{K_1/K} + \frac{M^{2\,\mathrm{free}}_{c\bar{c}}(N_2,K_2)}{K_2/K}\right], \quad (53)$$

where N_2 and K_2 are fixed by the conditions $N_1 + N_2 = N_{\max}$ and $K_1 + K_2 = K$. $M^{2\,\mathrm{free}}_{cc\bar{c}\,\bar{c}}$ and $M^{2\,\mathrm{free}}_{c\bar{c}}$ are tetraquark and meson ground-state masses squared, respectively, computed with all interactions turned off. We use masses squared instead of masses because they, and not the masses, are the eigenvalues of our Hamiltonian. Moreover, the two two-quark masses, $M^{2\mathrm{free}}_{c\bar{c}}(N_1,K_1)$ and $M^{2\mathrm{free}}_{c\bar{c}}(N_2,K_2)$, need to be combined according to Eq. (35) to get the invariant mass of the full state. To get the minimal invariant mass we put $\mathbf{k}_{AB} = 0$ and minimize over all possible values of N_1, N_2 and K_1, K_2 into which $N_{\max}$ and K can be partitioned. Hence, ΔM^2, being the difference between the actual tetraquark mass and the minimal possible mass of two separate two-quark subsystems, is a measure of minimal $\mathbf{k}_{AB}$ between the two subsystems. Table III lists the values that we obtain. Note that ΔM^2 does not depend on K for the choice of K's that we made. It should stay the same for all $K = 2 \pmod 4$. We correct the actual eigenvalues of the truncated Hamiltonians by subtracting the kinetic energy penalty,

TABLE III. Kinetic energy penalty in GeV^2.

$N_{\max}$	6	8	10	12
ΔM^2	1.213	1.013	0.659	0.584

$$M^{2\,\mathrm{corrected}}_{cc\bar{c}\,\bar{c}} = M^{2\,\mathrm{full}}_{cc\bar{c}\,\bar{c}}(N_{\max},K) - \Delta M^2(N_{\max},K). \quad (54)$$

To give an estimate for a typical downward shift of tetraquark masses introduced by this correction, for $N_{\max} = 12$, if $M^{\mathrm{full}}_{cc\bar{c}\,\bar{c}} = 6$ GeV, then $M^{\mathrm{full}}_{cc\bar{c}\,\bar{c}} - M^{\mathrm{corrected}}_{cc\bar{c}\,\bar{c}} \approx 49$ MeV.

We introduce three estimates of the threshold with which we compare our numerical tetraquark masses. One estimate uses the same idea behind the second term in Eq. (53) but with full meson masses that include interactions,

$$T'_1 = \sqrt{\min_{N_1,K_1}\left[\frac{M^{2\,\mathrm{full}}_{c\bar{c}}(N_1,K_1)}{K_1/K} + \frac{M^{2\,\mathrm{full}}_{c\bar{c}}(N_2,K_2)}{K_2/K}\right]}, \quad (55)$$

where the minimum, as in Eq. (53), is taken over all possible values of N_1 and K_1. Threshold T'_1 gives an unexpectedly poor estimate. It is substantially smaller than twice our fitted numerical mass of η_c. The reason seems to be an overestimation of the OGE potential for small values of K because the minima of T'_1 tend to be reached at the minimal $K_1 = 1$, while turning off the OGE potential makes the minima appear for $K_1 = K_2 = K/2$. In fact, one naively expects the minimum in the definition of T'_1 to be reached for $K_1 = K/2$ because it implies $x_A = x_B = 1/2$, which means zero relative longitudinal momentum between the two mesons (as long as they have equal masses). Moreover, the actual $M^{2\,\mathrm{full}}_{c\bar{c}}$ turns out to be negative for some $K = 1$ cases, which is unacceptable. Therefore, we define another estimate of the threshold, for which both $N_{\max}$ and K are equally partitioned among N_1, N_2 and K_1, K_2, i.e.,

$$T_1(N_{\max},K) = 2\sqrt{M^{2\,\mathrm{full}}_{c\bar{c}}\left(\frac{N_{\max}}{2},\frac{K}{2}\right)}. \quad (56)$$

This estimate seems to be more reasonable, and it is in rough agreement with a third estimate of the threshold provided below.

By turning off interactions between particles that do not belong to the same meson, we can compute the invariant mass of two mesons occupying almost the same

TABLE IV. Values (in MeV) of threshold estimates T_1, T_2 and corrected tetraquark masses $M^{\text{corrected}}_{cc\bar{c}\,\bar{c}}$ for various $N_{\max}$ and K.

K	6				10				14				18			
$N_{\max}$	6	8	10	12	6	8	10	12	6	8	10	12	6	8	10	12
T_1	5215	4832	4758	4565	5895	5662	5613	5484	6105	5987	5970	5918	6192	6100	6089	6060
T_2	4999	4754	4513	4093	5774	5598	5484	5372	6140	6032	5972	5903	6282	6208	6178	6140
$M^{\text{corrected}}_{cc\bar{c}\,\bar{c}}$	7810	7783	7787	7781	7659	7631	7637	7633	7600	7572	7578	7574	7567	7540	7546	7542

finite basis—we have to make identical particles distinguishable because otherwise one would not be able to consistently turn off, for example, an interaction between 1 and 4 and at the same time keep interaction between 1 and 3 turned on. Therefore, we define

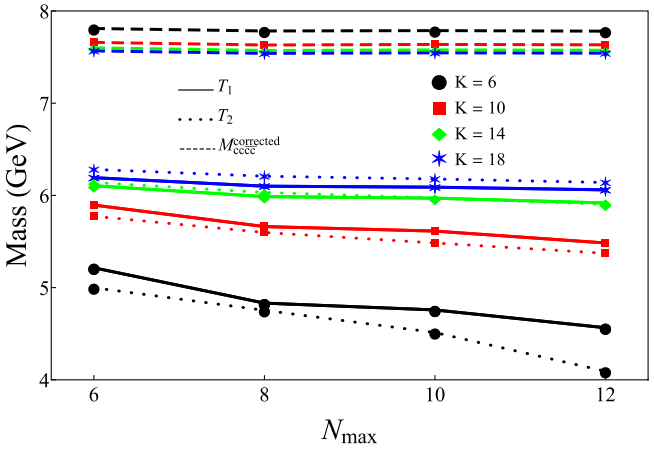

FIG. 1. Threshold estimates T_1, T_2 and tetraquark masses $M^{\text{corrected}}_{cc\bar{c}\,\bar{c}}$ depending on $N_{\max}$ and K. Dashed lines connect symbols representing $M^{\text{corrected}}_{cc\bar{c}\,\bar{c}}$, solid lines connect symbols representing T_1, and dotted lines connect symbols representing T_2. Different symbols represent different K. With an increasing K the threshold lines go up, while the tetraquark lines go down.

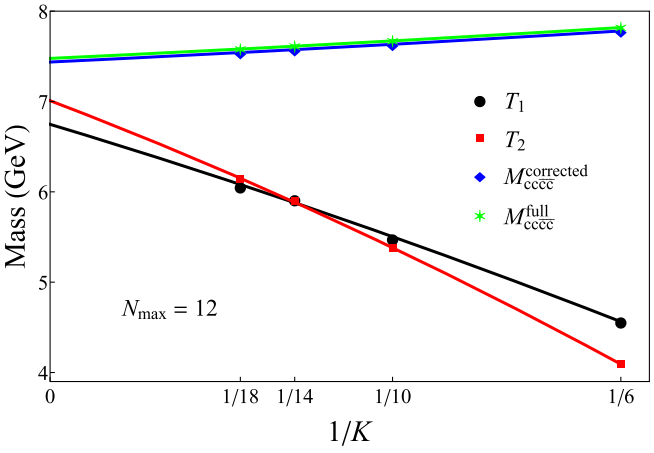

FIG. 2. Threshold estimates and tetraquark masses as functions of $1/K$ for $N_{\max} = 12$. The fitted solid lines (of the form $a + b/K + c/K^2$) are used to extrapolate the results to the point $1/K = 0$.

$$T_2 = \sqrt{M^2_{\text{two-meson}}(N_{\max}, K) - \Delta M^2(N_{\max}, K)}, \quad (57)$$

where $M^2_{\text{two-meson}}$ is the ground-state mass in the aforementioned calculation of a two-meson system in a tetraquark calculation. The results for threshold estimates and tetraquark masses are summarized in Table IV and plotted in Fig. 1.

Figure 2 shows the result of a least squares fit of $a + b/K + c/K^2$ to threshold estimates and tetraquark masses for $N_{\max} = 12$. The results for parameter a, i.e., extrapolations of the fitted curves to the point $1/K = 0$ are $T_1 = (6748 \pm 225)$ MeV, $T_2 = (7009 \pm 111)$ MeV, $M^{\text{full}}_{cc\bar{c}\,\bar{c}} = (7477 \pm 2)$ MeV, and $M^{\text{corrected}}_{cc\bar{c}\,\bar{c}} = (7438 \pm 2)$ MeV. All those numbers are expected to go down in the limit $N_{\max} \to \infty$ (provided that we do not refit our meson masses), but we expect that the shift should be much smaller than the shift due to $K \to \infty$ extrapolation. Our gluon mass introduces an additional shift upward on the order of the value of μ, i.e., 10 MeV. All tetraquark masses lie substantially above all threshold estimates, including the extrapolations. These results indicate that the lowest $cc\bar{c}\,\bar{c}$ eigenstate of our model Hamiltonian is not bound with respect to breakup into two separated mesons. It could be a resonant state. However, such a conclusion would require additional confirmation in the form of a decay analysis.

V. CONCLUSION

We have done, to our knowledge, the first study of all-heavy tetraquark states using a Hamiltonian in the front form of dynamics, where all quarks are treated individually, color degrees of freedom are unconstrained (apart from the restriction to global color singlets), and antisymmetrizations due to identical particles are taken into account.

We note, however, that our confining potential breaks the cluster decomposition principle, but the breaking should be rather small for a nonrelativistic system like an all-charm tetraquark. Attempts to restore it exactly lead to unphysical states with negative mass squared. Therefore, our confining potential should be regarded as an approximate effective potential with a limited range of applicability.

Even without the negative M^2 problem, confining long-range forces lead to problematic long-range van der Waals forces [72,73]. Such long-range forces are unlikely to be present in QCD. A more likely picture would involve

effective, massive gluons to be the source of confining forces. They may or may not form strings, but in any case a force mediated by such gluons would be short-range.

All our estimates for the $cc\bar{c}\,\bar{c}$ ground-state mass turn out to be substantially higher than the estimates we made for the lowest threshold for breakup into two $c\bar{c}$ mesons. Therefore, in our model, the ground-state tetraquark is unstable against dissociation into two charmonia. There remain, however, open questions. For example, what would happen if we used much larger basis spaces? Our estimates seem to indicate a gap between the two-meson threshold and the lowest tetraquark, but ultimately, close to the threshold, we should see a lot of states filling a continuum spectrum. We might also see some molecular states bound by the van der Waals forces. The 15% color-independent admixture might play a role here because it is, perhaps a bit counterintuitively, likely to work against the binding of tetraquark states. This is because all pairs of quarks in a tetraquark contribute an upward shift of mass due to zero-point energy, while for the OGE-like case four of the potentials cancel each other to a large extent in the color configuration with two color singlets. At the same time, by design, meson spectra and two-meson spectra are unaffected by the admixture.

Even if the ground-state tetraquark is unstable, there may still be stable tetraquarks higher in the mass, because their thresholds can be higher. For example, Barnea *et al.* [7], using hyperspherical expansion to solve the Schrödinger equation, find exotic states 0^{+-} (6515 MeV) and 2^{+-} (6586 MeV) to be substantially below their respective thresholds for dissociation.

It is also worth noting that the results for tetraquark masses seem to be much more reliable than the threshold estimates that we obtain, as can be seen in Fig. 2 and in our extrapolations. Fit uncertainties are very small for tetraquarks, and very large for threshold estimates. This is fortunate because meson calculations require far less amount of computational resources, and hence can be straightforwardly improved. Therefore, we could fit parameters using the extrapolations $K \to \infty$ and $N_{\max} \to \infty$ of meson masses (instead of at fixed K and $N_{\max}$). This would give us the threshold at physical values, while extrapolations of tetraquark masses from comparatively smaller K and $N_{\max}$ would still give reliable results.

ACKNOWLEDGMENTS

K. S. is supported by the Chinese Academy of Sciences President's International Fellowship Initiative (PIFI), Grant No. 2021PM0066, the Chinese Ministry of Science and Technology Foreign Expert Project, Grant No. QN20200143003, and the National Natural Science Foundation of China (NSFC) under Grant No. 12047555. Z. K. and X. Z. are supported by new faculty start-up funding by the Institute of Modern Physics, Chinese Academy of Sciences, by Key Research Program of Frontier Sciences, Chinese Academy of Sciences, Grant No. ZDB-SLY-7020, by the Natural Science Foundation of Gansu Province, China, Grant No. 20JR10RA067, by the Foundation for Key Talents of Gansu Province, and by Strategic Priority Research Program of the Chinese Academy of Sciences Grant No. XDB34000000. This material is based upon work supported by the U.S. Department of Energy, Office of Science, under Awards No. DE-FG02-87ER40371 and No. DE-SC0018223 (SciDAC4/NUCLEI). This research used the computing resources of Gansu Computing Center and Gansu Advanced Computing Center.

APPENDIX: ANTISYMMETRIZATION OF THE BASIS AND COLOR PROJECTION

The color space for two quarks and two antiquarks is $3^4 = 81$ dimensional. Assuming color confinement, only color-singlet states can be physically realized. The space of $QQ\bar{Q}\,\bar{Q}$ color-singlet states is only two dimensional. It is, therefore, worth working with color-singlet states only because that means that the matrices that need to be diagonalized numerically have, roughly speaking, 40 times smaller dimensions. We refer the reader to Fig. 12 in Ref. [42] for detailed examples of numbers of color singlets in sectors with more particles. One has to invest, however, extra effort in the evaluation of the matrix elements of the Hamiltonian.

The first step, which needs to be taken in any case, is to define a space of states with arbitrary color that takes into account the fact that some particles are identical. One can use states

$$|1234\rangle = B_1^\dagger B_2^\dagger D_3^\dagger D_4^\dagger |0\rangle. \tag{A1}$$

Each particle is characterized by five quantum numbers: k_i, longitudinal momentum number; n_i, transverse-harmonic-oscillator radial number; m_i, transverse-harmonic-oscillator angular number; σ_i, light-front helicity; c_i, color, with $i = 1, 2, 3, 4$. For each state $|1234\rangle$ there are several other states that are linearly dependent, e.g., $|2134\rangle = -|1234\rangle$ and $|1243\rangle = -|1234\rangle$. Moreover, some states are identically zero, e.g., $|1134\rangle = 0$. To define a proper orthonormal basis one has to constrain possible quantum numbers of the particles. Since quarks are fermions, this can be done using a relation of strict order. We say that $1 > 2$ if and only if $k_1 > k_2$, or $k_1 = k_2$ and $n_1 > n_2$, or $k_1 = k_2$ and $n_1 = n_2$ and $m_1 > m_2$, or $k_1 = k_2$ and $n_1 = n_2$ and $m_1 = m_2$ and $\sigma_1 > \sigma_2$, or $k_1 = k_2$ and $n_1 = n_2$ and $m_1 = m_2$ and $\sigma_1 = \sigma_2$ and $c_1 > c_2$. We define our basis to contain only such states $|1234\rangle$ for which $1 > 2$ and $3 > 4$. Taking another such state $|1'2'3'4'\rangle$ with $1' > 2'$ and $3' > 4'$, we have $\langle 1234|1'2'3'4'\rangle = \delta_{11'}\delta_{22'}\delta_{33'}\delta_{44'}$, where $\delta_{ij} = \delta_{k_i,k_j}\delta_{n_i,n_j}\delta_{m_i,m_j}\delta_{\sigma_i,\sigma_j}\delta_{c_i,c_j}$.

For the second step we need to find color-singlet states, which are defined as the kernel of the quadratic Casimir operator $C_2 = \sum_{a=1}^{8} \hat{T}^a \hat{T}^a$, where

$$\hat{T}^a = \sum_{12} \delta_{k_1,k_2}\delta_{n_1,n_2}\delta_{m_1,m_2}\delta_{\sigma_1,\sigma_2}(t^a_{c_1c_2}B_1^\dagger B_2 - t^a_{c_2c_1}D_1^\dagger D_2), \tag{A2}$$

where $\sum_{12}$ is the sum over all quantum numbers of particles 1 and 2. We omit the gluon part because we do not have gluons in our model. The color operators $\hat{T}^a$ do not change any of the momentum and spin quantum numbers; hence, C_2 is diagonal in momentum and spin. Therefore, we can separately diagonalize C_2 in subspaces of fixed momentum and spin quantum numbers. Note that our relation $i > j$ compares colors c_i and c_j in the very end only if all the other quantum numbers turned out to be the same.

There are four different kinds of subspaces. To classify them, it is convenient to introduce another two relations. We say that $i \approx j$ if all quantum numbers of i and j except color are the same (colors can be arbitrary). We say that $i \gg j$ if $i > j$ and not $i \approx j$. In other words, either $k_i > k_j$ or $k_i = k_j$ and $n_i > n_j$, or $k_i = k_j$ and $n_i = n_j$ and $m_i > m_j$, or $k_i = k_j$ and $n_i = n_j$ and $m_i = m_j$ and $\sigma_i > \sigma_j$. Hence, the symbol $\gg$ is just like $>$ except that it does not take color into account. We can now easily classify the four cases of color spaces.

Case 1: $1 \gg 2$ and $3 \gg 4$. In this case all 81 color combinations are allowed. The color-singlet subspace is two dimensional and spanned by

$$\begin{aligned}|1234, S\rangle = \frac{1}{2\sqrt{6}}(&2|rr\bar{r}\,\bar{r}\rangle + 2|gg\bar{g}\,\bar{g}\rangle + 2|bb\bar{b}\,\bar{b}\rangle \\ &+ |rg\bar{r}\,\bar{g}\rangle + |gr\bar{r}\,\bar{g}\rangle + |gr\bar{g}\,\bar{r}\rangle + |rg\bar{g}\,\bar{r}\rangle \\ &+ |gb\bar{g}\,\bar{b}\rangle + |bg\bar{g}\,\bar{b}\rangle + |bg\bar{b}\,\bar{g}\rangle + |gb\bar{b}\,\bar{g}\rangle \\ &+ |br\bar{b}\,\bar{r}\rangle + |rb\bar{b}\,\bar{r}\rangle + |rb\bar{r}\,\bar{b}\rangle + |br\bar{r}\,\bar{b}\rangle),\end{aligned} \tag{A3}$$

$$\begin{aligned}|1234, A_1\rangle = \frac{1}{\sqrt{12}}(&|rg\bar{r}\,\bar{g}\rangle - |gr\bar{r}\,\bar{g}\rangle + |gr\bar{g}\,\bar{r}\rangle - |rg\bar{g}\,\bar{r}\rangle \\ &+ |gb\bar{g}\,\bar{b}\rangle - |bg\bar{g}\,\bar{b}\rangle + |bg\bar{b}\,\bar{g}\rangle - |gb\bar{b}\,\bar{g}\rangle \\ &+ |br\bar{b}\,\bar{r}\rangle - |rb\bar{b}\,\bar{r}\rangle + |rb\bar{r}\,\bar{b}\rangle - |br\bar{r}\,\bar{b}\rangle),\end{aligned} \tag{A4}$$

where kets on the right-hand sides are denoted by colors $|c_1c_2c_3c_4\rangle$ and we omit momentum and spin quantum numbers, which are the same for each ket. Instead of 1, 2, 3, colors are called r, g, b, respectively, for quarks and $\bar{r}$, $\bar{g}$, $\bar{b}$, respectively, for antiquarks. For completeness, $r < g < b$ and $\bar{r} < \bar{g} < \bar{b}$. Note that $|1234, S\rangle$ is symmetric for either $1 \leftrightarrow 2$ or $3 \leftrightarrow 4$, while $|1234, A_1\rangle$ is antisymmetric for either $1 \leftrightarrow 2$ or $3 \leftrightarrow 4$.

Case 2: $1 \approx 2$ and $3 \gg 4$. Now only three quark-quark color combinations, bg, br, and gr, are allowed (because $1 > 2$ still holds), while the colors of antiquarks are unconstrained. Therefore, this color space is 27 dimensional and there is only one antisymmetric color-singlet combination,

$$\begin{aligned}|1234, A_2\rangle = \frac{1}{\sqrt{6}}(&|gr\bar{g}\,\bar{r}\rangle - |gr\bar{r}\,\bar{g}\rangle + |br\bar{b}\,\bar{r}\rangle \\ &- |br\bar{r}\,\bar{b}\rangle + |bg\bar{b}\,\bar{g}\rangle - |bg\bar{g}\,\bar{b}\rangle).\end{aligned} \tag{A5}$$

Case 3: $1 \gg 2$ and $3 \approx 4$. In analogy with case 2, only three antiquark-antiquark color combinations, $\bar{b}\,\bar{g}$, $\bar{b}\,\bar{r}$, and $\bar{g}\,\bar{r}$, are allowed because $3 > 4$, while the colors of quarks are unconstrained. The color space is again 27 dimensional and there is only one antisymmetric color-singlet combination,

$$\begin{aligned}|1234, A_3\rangle = \frac{1}{\sqrt{6}}(&|gr\bar{g}\,\bar{r}\rangle - |rg\bar{g}\,\bar{r}\rangle + |br\bar{b}\,\bar{r}\rangle \\ &- |rb\bar{b}\,\bar{r}\rangle + |bg\bar{b}\,\bar{g}\rangle - |gb\bar{b}\,\bar{g}\rangle).\end{aligned} \tag{A6}$$

Case 4: $1 \approx 2$ and $3 \approx 4$. Both quarks and antiquarks have constrained colors because $1 > 2$ and $3 > 4$. The color space is nine dimensional and there is only one antisymmetric color-singlet combination,

$$|1234, A_4\rangle = \frac{1}{\sqrt{3}}(|gr\bar{g}\,\bar{r}\rangle + |br\bar{b}\,\bar{r}\rangle + |bg\bar{b}\,\bar{g}\rangle). \tag{A7}$$

The third and last step is to calculate the common factors in Hamiltonian matrix elements between states with different color-singlet configurations that arise due to color and antisymmetrization. We summarize the results. In general we need to evaluate matrix elements of the following types of operators,

$$\hat{V}_q = \sum_{5',5} \delta_{c_{5'},c_5} V_{5';5} B^\dagger_{5'} B_5, \tag{A8}$$

$$\hat{V}_{\bar{q}} = \sum_{5',5} \delta_{c_{5'},c_5} V_{5';5} D^\dagger_{5'} D_5, \tag{A9}$$

$$\hat{V}_{qq} = \sum_{5',6',5,6} C^{qq}_{5',6';5,6} V_{5',6';5,6} \frac{1}{2} B^\dagger_{5'} B^\dagger_{6'} B_6 B_5, \tag{A10}$$

$$\hat{V}_{\bar{q}\,\bar{q}} = \sum_{5',6',5,6} C^{\bar{q}\,\bar{q}}_{5',6';5,6} V_{5',6';5,6} \frac{1}{2} D^\dagger_{5'} D^\dagger_{6'} D_6 D_5, \tag{A11}$$

$$\hat{V}_{q\bar{q}} = \sum_{5',6',5,6} C^{q\bar{q}}_{5',6';5,6} V_{5',6';5,6} B^\dagger_{5'} D^\dagger_{6'} D_6 B_5, \tag{A12}$$

TABLE V. Interaction color factors between color-singlet states.

			Color independent			OGE-like		
IJ	C_{IJ}^{q}	$C_{IJ}^{\bar{q}}$	C_{IJ}^{qq}	$C_{IJ}^{\bar{q}\,\bar{q}}$	$C_{IJ}^{q\bar{q}}$	C_{IJ}^{qq}	$C_{IJ}^{\bar{q}\,\bar{q}}$	$C_{IJ}^{q\bar{q}}$
SS	1	1	$\frac{1}{2}$	$\frac{1}{2}$	1	$\frac{1}{6}$	$\frac{1}{6}$	$-\frac{5}{6}$
SA_j or A_iS	0	0	0	0	0	0	0	$-\frac{1}{\sqrt{2}}$
A_iA_j	1	1	$\frac{1}{2}$	$\frac{1}{2}$	1	$-\frac{1}{3}$	$-\frac{1}{3}$	$-\frac{1}{3}$

where $V_{5';5}$ and $V_{5',6';5,6}$ depend on all quantum numbers except color, while $C^{qq}_{5',6';5,6}$, $C^{\bar{q}\,\bar{q}}_{5',6';5,6}$, and $C^{q\bar{q}}_{5',6';5,6}$ depend only on color. There are two types of interactions: color-independent ones, for which

$$C^{qq}_{5',6';5,6} = C^{\bar{q}\,\bar{q}}_{5',6';5,6} = C^{q\bar{q}}_{5',6';5,6} = \delta_{c_{5'},c_5}\delta_{c_{6'},c_6}, \tag{A13}$$

and OGE-like interactions, for which

$$C^{qq}_{5',6';5,6} = \sum_{a=1}^{8} t^a_{5'5} t^a_{6'6}, \tag{A14}$$

$$C^{\bar{q}\,\bar{q}}_{5',6';5,6} = \sum_{a=1}^{8} t^a_{55'} t^a_{66'}, \tag{A15}$$

$$C^{q\bar{q}}_{5',6';5,6} = -\sum_{a=1}^{8} t^a_{5'5} t^a_{66'}. \tag{A16}$$

Note that $C^{qq}_{5',6';5,6} = C^{\bar{q}\,\bar{q}}_{5',6';5,6}$. We label color singlets with capital letters I and J that can equal S, A_1, A_2, A_3, or A_4. The general matrix elements are

$$\langle 1'2'3'4', I|\hat{V}_q|1234, J\rangle = C^q_{IJ} S^q_I S^q_J V^q_{IJ} \delta_{e_{3'},e_3}\delta_{e_{4'},e_4}, \tag{A17}$$

$$\langle 1'2'3'4', I|\hat{V}_{\bar{q}}|1234, J\rangle = C^{\bar{q}}_{IJ} S^{\bar{q}}_I S^{\bar{q}}_J V^{\bar{q}}_{IJ} \delta_{e_{1'},e_1}\delta_{e_{2'},e_2}, \tag{A18}$$

$$\langle 1'2'3'4', I|\hat{V}_{qq}|1234, J\rangle = C^{qq}_{IJ} S^q_I S^q_J V^{qq}_{IJ} \delta_{e_{3'},e_3}\delta_{e_{4'},e_4}, \tag{A19}$$

$$\langle 1'2'3'4', I|\hat{V}_{\bar{q}\,\bar{q}}|1234, J\rangle = C^{\bar{q}\,\bar{q}}_{IJ} S^{\bar{q}}_I S^{\bar{q}}_J V^{\bar{q}\,\bar{q}}_{IJ} \delta_{e_{1'},e_1}\delta_{e_{2'},e_2}, \tag{A20}$$

$$\langle 1'2'3'4', I|\hat{V}_{q\bar{q}}|1234, J\rangle = C^{q\bar{q}}_{IJ} S^{q\bar{q}}_I S^{q\bar{q}}_J V^{q\bar{q}}_{IJ}, \tag{A21}$$

where e_i stands for all quantum numbers of particle i except color, i.e., n_i, m_i, k_i, and σ_i. Hence, δ_{e_i,e_j} is a product of four Kronecker deltas, $\delta_{k_i,k_j}\delta_{n_i,n_j}\delta_{m_i,m_j}\delta_{\sigma_i,\sigma_j}$. The color factors C_{IJ} are given in Table V. The symmetry factors S_I are given in Table VI. Finally, the V factors are

TABLE VI. Symmetry factors S_I as functions of I. Note that $S^{q\bar{q}}_I = S^q_I S^{\bar{q}}_I$.

I	S^q_I	$S^{\bar{q}}_I$	$S^{q\bar{q}}_I$
S	1	1	1
A_1	1	1	1
A_2	$\frac{1}{\sqrt{2}}$	1	$\frac{1}{\sqrt{2}}$
A_3	1	$\frac{1}{\sqrt{2}}$	$\frac{1}{\sqrt{2}}$
A_4	$\frac{1}{\sqrt{2}}$	$\frac{1}{\sqrt{2}}$	$\frac{1}{2}$

$$V^q_{SS} = V_{1';1}\delta_{e_{2'},e_2} - V_{1';2}\delta_{e_{2'},e_1} - V_{2';1}\delta_{e_{1'},e_2} + V_{2';2}\delta_{e_{1'},e_1}, \tag{A22}$$

$$V^q_{A_iA_j} = V_{1';1}\delta_{e_{2'},e_2} + V_{1';2}\delta_{e_{2'},e_1} + V_{2';1}\delta_{e_{1'},e_2} + V_{2';2}\delta_{e_{1'},e_1}, \tag{A23}$$

$$V^{\bar{q}}_{SS} = V_{3';3}\delta_{e_{4'},e_4} - V_{3';4}\delta_{e_{4'},e_3} - V_{4';3}\delta_{e_{3'},e_4} + V_{4';4}\delta_{e_{3'},e_3}, \tag{A24}$$

$$V^{\bar{q}}_{A_iA_j} = V_{3';3}\delta_{e_{4'},e_4} + V_{3';4}\delta_{e_{4'},e_3} + V_{4';3}\delta_{e_{3'},e_4} + V_{4';4}\delta_{e_{3'},e_3}, \tag{A25}$$

$$V^{qq}_{SS} = V_{1',2';1,2} - V_{2',1';1,2} - V_{1',2';2,1} + V_{2',1';2,1}, \tag{A26}$$

$$V^{qq}_{A_iA_j} = V_{1',2';1,2} + V_{2',1';1,2} + V_{1',2';2,1} + V_{2',1';2,1}, \tag{A27}$$

$$V^{\bar{q}\,\bar{q}}_{SS} = V_{3',4';3,4} - V_{4',3';3,4} - V_{3',4';4,3} + V_{4',3';4,3}, \tag{A28}$$

$$V^{\bar{q}\,\bar{q}}_{A_iA_j} = V_{3',4';3,4} + V_{4',3';3,4} + V_{3',4';4,3} + V_{4',3';4,3}, \tag{A29}$$

$$\begin{aligned} V^{q\bar{q}}_{IJ} = [&V_{1',3';1,3} + aV_{1',4';1,3} + aV_{2',3';1,3} + V_{2',4';1,3} \\ &+ bV_{1',3';1,4} + abV_{1',4';1,4} + abV_{2',3';1,4} + bV_{2',4';1,4} \\ &+ bV_{1',3';2,3} + abV_{1',4';2,3} + abV_{2',3';2,3} + bV_{2',4';2,3} \\ &+ V_{1',3';2,4} + aV_{1',4';2,4} + aV_{2',3';2,4} + V_{2',4';2,4}]\widetilde{\delta\delta}, \end{aligned} \tag{A30}$$

where $a = -1$ if $I = S$ and $a = 1$ if $I = A_i$, while $b = -1$ if $J = S$ and $b = 1$ if $J = A_j$. $\widetilde{\delta\delta}$ stands for matching Kronecker deltas in quantum numbers of the spectators of the interaction, and it is different for each of the 16 terms in Eq. (A30). For example, $V_{2',4';1,3}$ describes an interaction where the final interacting quark-antiquark pair is $2'4'$, while initial interacting quark-antiquark pair is 13. Hence, the final spectator quark-antiquark pair is $1'3'$ and the initial

spectator quark-antiquark pair is 24. Therefore, $\widetilde{\delta\delta} = \delta_{e_{1'},e_2}\delta_{e_{3'},e_4}$ in this case. V^q, $V^{\bar{q}}$, V^{qq}, and $V^{\bar{q}\bar{q}}$ need not be defined for $IJ = SA_j$ or A_iS, because color factors are always zero in those cases. It is also worth noting that if $I \in \{A_3, A_4\}$ and $J \in \{S, A_1, A_2\}$ or if $J \in \{A_3, A_4\}$ and $I \in \{S, A_1, A_2\}$, then $\delta_{e_{3'},e_3}\delta_{e_{4'},e_4}$ is always zero. Similarly, if $I \in \{A_2, A_4\}$ and $J \in \{S, A_1, A_3\}$ or if $J \in \{A_2, A_4\}$ and $I \in \{S, A_1, A_3\}$, then $\delta_{e_{1'},e_1}\delta_{e_{2'},e_2}$ is always zero.

[1] Y. Iwasaki, Prog. Theor. Phys. **54**, 492 (1975).
[2] R. L. Jaffe, Phys. Rev. D **15**, 267 (1977).
[3] J. P. Ader, J. M. Richard, and P. Taxil, Phys. Rev. D **25**, 2370 (1982).
[4] L. Heller and J. A. Tjon, Phys. Rev. D **32**, 755 (1985).
[5] Y.-R. Liu, H.-X. Chen, W. Chen, X. Liu, and S.-L. Zhu, Prog. Part. Nucl. Phys. **107**, 237 (2019).
[6] R. J. Lloyd and J. P. Vary, Phys. Rev. D **70**, 014009 (2004).
[7] N. Barnea, J. Vijande, and A. Valcarce, Phys. Rev. D **73**, 054004 (2006).
[8] A. V. Berezhnoy, A. V. Luchinsky, and A. A. Novoselov, Phys. Rev. D **86**, 034004 (2012).
[9] W. Heupel, G. Eichmann, and C. S. Fischer, Phys. Lett. B **718**, 545 (2012).
[10] Y. Bai, S. Lu, and J. Osborne, Phys. Lett. B **798**, 134930 (2019).
[11] W. Chen, H.-X. Chen, X. Liu, T. G. Steele, and S.-L. Zhu, Phys. Lett. B **773**, 247 (2017).
[12] M. Karliner, S. Nussinov, and J. L. Rosner, Phys. Rev. D **95**, 034011 (2017).
[13] J. Wu, Y.-R. Liu, K. Chen, X. Liu, and S.-L. Zhu, Phys. Rev. D **97**, 094015 (2018).
[14] M. N. Anwar, J. Ferretti, F.-K. Guo, E. Santopinto, and B.-S. Zou, Eur. Phys. J. C **78**, 647 (2018).
[15] V. R. Debastiani and F. S. Navarra, Chin. Phys. C **43**, 013105 (2019).
[16] J.-M. Richard, A. Valcarce, and J. Vijande, Phys. Rev. D **95**, 054019 (2017).
[17] A. Esposito and A. D. Polosa, Eur. Phys. J. C **78**, 782 (2018).
[18] J.-M. Richard, A. Valcarce, and J. Vijande, Phys. Rev. C **97**, 035211 (2018).
[19] Z.-G. Wang and Z.-Y. Di, Acta Phys. Pol. B **50**, 1335 (2019).
[20] M. A. Bedolla, J. Ferretti, C. D. Roberts, and E. Santopinto, Eur. Phys. J. C **80**, 1004 (2020).
[21] M.-S. Liu, Q.-F. Lü, X.-H. Zhong, and Q. Zhao, Phys. Rev. D **100**, 016006 (2019).
[22] G.-J. Wang, L. Meng, and S.-L. Zhu, Phys. Rev. D **100**, 096013 (2019).
[23] R. M. Albuquerque, S. Narison, A. Rabemananjara, D. Rabetiarivony, and G. Randriamanatrika, Phys. Rev. D **102**, 094001 (2020).
[24] H.-X. Chen, W. Chen, X. Liu, and S.-L. Zhu, Sci. Bull. **65**, 1994 (2020).
[25] C. Deng, H. Chen, and J. Ping, Phys. Rev. D **103**, 014001 (2021).
[26] X.-K. Dong, V. Baru, F.-K. Guo, C. Hanhart, and A. Nefediev, Phys. Rev. Lett. **126**, 132001 (2021); **127**, 119901(E) (2021).
[27] H. Garcilazo and A. Valcarce, Eur. Phys. J. C **80**, 720 (2020).
[28] J. F. Giron and R. F. Lebed, Phys. Rev. D **102**, 074003 (2020).
[29] M. C. Gordillo, F. De Soto, and J. Segovia, Phys. Rev. D **102**, 114007 (2020).
[30] X. Jin, Y. Xue, H. Huang, and J. Ping, Eur. Phys. J. C **80**, 1083 (2020).
[31] M. Karliner and J. L. Rosner, Phys. Rev. D **102**, 114039 (2020).
[32] P. Lundhammar and T. Ohlsson, Phys. Rev. D **102**, 054018 (2020).
[33] R. Maciuła, W. Schäfer, and A. Szczurek, Phys. Lett. B **812**, 136010 (2021).
[34] L. Maiani, Sci. Bull. **65**, 1949 (2020).
[35] J.-M. Richard, Sci. Bull. **65**, 1954 (2020).
[36] J. Sonnenschein and D. Weissman, Eur. Phys. J. C **81**, 25 (2021).
[37] Z.-G. Wang, Int. J. Mod. Phys. A **36**, 2150014 (2021).
[38] X.-Y. Wang, Q.-Y. Lin, H. Xu, Y.-P. Xie, Y. Huang, and X. Chen, Phys. Rev. D **102**, 116014 (2020).
[39] X.-Z. Weng, X.-L. Chen, W.-Z. Deng, and S.-L. Zhu, Phys. Rev. D **103**, 034001 (2021).
[40] J.-R. Zhang, Phys. Rev. D **103**, 014018 (2021).
[41] P. A. M. Dirac, Rev. Mod. Phys. **21**, 392 (1949).
[42] J. P. Vary, H. Honkanen, J. Li, P. Maris, S. J. Brodsky, A. Harindranath, G. F. de Teramond, P. Sternberg, E. G. Ng, and C. Yang, Phys. Rev. C **81**, 035205 (2010).
[43] R. Aaij *et al.* (LHCb Collaboration), Sci. Bull. **65**, 1983 (2020).
[44] R. Aaij *et al.* (LHCb Collaboration), arXiv:2109.01038.
[45] Y. Li, P. Maris, X. Zhao, and J. P. Vary, Phys. Lett. B **758**, 118 (2016).
[46] Y. Li, P. Maris, and J. P. Vary, Phys. Rev. D **96**, 016022 (2017).
[47] S. Jia and J. P. Vary, Phys. Rev. C **99**, 035206 (2019).
[48] S. Tang, Y. Li, P. Maris, and J. P. Vary, Eur. Phys. J. C **80**, 522 (2020).
[49] J. Lan, C. Mondal, S. Jia, X. Zhao, and J. P. Vary, Phys. Rev. Lett. **122**, 172001 (2019).
[50] J. Lan, C. Mondal, S. Jia, X. Zhao, and J. P. Vary, Phys. Rev. D **101**, 034024 (2020).
[51] C. Mondal, S. Xu, J. Lan, X. Zhao, Y. Li, D. Chakrabarti, and J. P. Vary, Phys. Rev. D **102**, 016008 (2020).

[52] J. Lan, C. Mondal, M. Li, Y. Li, S. Tang, X. Zhao, and J. P. Vary, Phys. Rev. D **102**, 014020 (2020).
[53] S. Xu, C. Mondal, J. Lan, X. Zhao, Y. Li, and J. P. Vary (BLFQ Collaboration), Phys. Rev. D **104**, 094036 (2021).
[54] W. Qian, S. Jia, Y. Li, and J. P. Vary, Phys. Rev. C **102**, 055207 (2020).
[55] P. Wiecki, Y. Li, X. Zhao, P. Maris, and J. P. Vary, Phys. Rev. D **91**, 105009 (2015).
[56] J. Lan, K. Fu, C. Mondal, X. Zhao, and J. P. Vary (BLFQ Collaboration), Phys. Lett. B **825**, 136890 (2022).
[57] S. D. Glazek, Acta Phys. Pol. B **43**, 1843 (2012).
[58] S. D. Glazek and M. Wieckowski, Phys. Rev. D **66**, 016001 (2002).
[59] S. D. Glazek and K. G. Wilson, Phys. Rev. D **48**, 5863 (1993).
[60] F. Wegner, Ann. Phys. (N.Y.) **506**, 77 (1994).
[61] S. Binder, J. Langhammer, A. Calci, P. Navratil, and R. Roth, Phys. Rev. C **87**, 021303(R) (2013).
[62] E. D. Jurgenson, P. Maris, R. J. Furnstahl, P. Navratil, W. E. Ormand, and J. P. Vary, Phys. Rev. C **87**, 054312 (2013).
[63] E. Gebrerufael, K. Vobig, H. Hergert, and R. Roth, Phys. Rev. Lett. **118**, 152503 (2017).
[64] S. J. Brodsky, H.-C. Pauli, and S. S. Pinsky, Phys. Rep. **301**, 299 (1998).
[65] S. J. Brodsky, G. F. de Teramond, H. G. Dosch, and J. Erlich, Phys. Rep. **584**, 1 (2015).
[66] A. P. Trawiński, S. D. Głazek, S. J. Brodsky, G. F. de Téramond, and H. G. Dosch, Phys. Rev. D **90**, 074017 (2014).
[67] Y. Aharonov, A. Komar, and L. Susskind, Phys. Rev. **182**, 1400 (1969).
[68] S. D. Głazek, M. Gómez-Rocha, J. More, and K. Serafin, Phys. Lett. B **773**, 172 (2017).
[69] K. Serafin, M. Gómez-Rocha, J. More, and S. D. Głazek, Eur. Phys. J. C **78**, 964 (2018).
[70] F. Coester and W. N. Polyzou, Phys. Rev. D **26**, 1348 (1982).
[71] J. P. Vary, L. Adhikari, G. Chen, S. Jia, M. Li, Y. Li, P. Maris, W. Qian, J. R. Spence, and S. Tang, Few-Body Syst. **59**, 56 (2018).
[72] O. W. Greenberg and H. J. Lipkin, Nucl. Phys. **A370**, 349 (1981).
[73] K. F. Liu, Phys. Lett. **131B**, 195 (1983).